OPEN

Correspondence and requests for materials should be addressed to G.U.K. (kulkarni@jncasr.ac.in)

Highly tapered pentagonal bipyramidal Au microcrystals with high index faceted corrugation: Synthesis and optical properties

Gangaiah Mettela[1], Radha Boya[1], Danveer Singh[2], G. V. Pavan Kumar[2] & G. U. Kulkarni[1]

[1]Chemistry and Physics of Materials Unit and DST Unit on Nanoscience, Jawaharlal Nehru Centre for Advanced Scientific Research, Jakkur P. O., Bangalore 560 064, India, [2]Photonics and Optical Nanoscopy Laboratory, Department of Physics and Chemistry, Indian Institute of Science Education and Research (IISER), Pune – 411008, India.

Focusing light at sub-wavelength region opens up interesting applications in optical sensing and imaging beyond the diffraction limit. In the past, tapered Au wires with carved gratings have been employed to achieve nanofocusing. The fabrication process however, is expensive and the obtained wires are polycrystalline with high surface roughness. A chemical synthetic method overcoming these hurdles should be an attractive alternative. Here, we report a method to chemically synthesize Au microcrystals ($\sim$10 μm) bearing pentagonal bipyramidal morphology with surface corrugations assignable to high index planes. The method is a single step solid state synthesis at a temperature amenable to common substrates. The microcrystals are tapered at both ends forming sharp tips ($\sim$55 nm). Individual microcrystals have been used as *pick and probe* SERS substrates for a dye embedded in a polymer matrix. The unique geometry of the microcrystal also enables light propagation across its length.

O ne-dimensional (1D) metal nanostructures have gained importance over the last decade due to their interesting optical properties such as tunable absorption from visible to near infrared region[1] and Raman scattering[2]. They exhibit distinct surface plasmon features, transverse and longitudinal, associated with their dimensionality[3] which is routinely observed with Ag and Au nanowires[4]. Apart from nanowires, there are other quasi 1D structures namely bipyramids or nanorice, bulged in the center and tapered at the ends[5], which have been the focus of recent research on anisotropic structures. For instance, Liu et al. have reported the synthesis of Au bipyramids with lengths of $\sim$120 nm prepared in a highly acidic medium[6]. Zheng et al. have synthesized Au nanorice (50–70 nm) bound by high index planes and utilized them for carbon monoxide oxidation[7]. Additionally, Au bipyramids have been employed in varied applications such as dampening of acoustic vibrations[8] and dielectric sensing[9]. Au nanostars with sharp tips have shown superior surface enhanced Raman spectroscopy (SERS) activity[10] and plasmon mediated sensing[11]. Odom and co-workers have shown the photothermal response of the Au nanopyramids with sharp tips[12]. Nanorice-like structures have been reported in the case of Ag as well[13]. Recently, star-fruit shaped Au nanorods of lengths up to $\sim$1 μm have been reported by Vigderman and co-workers[14]. However in such cases[15], the structures obtained are usually not beyond $\sim$1 μm (for a comprehensive survey of the current literature on bipyramids, see Supplementary Table S1 online). For many applications such as optical nano-focusing[16,17], it is desirable to have nanowire-like lengths, i.e., typically few micrometers but with the aforementioned special morphology. This explains the reason why many have resorted to using lithography methods to obtain large metal anisotropic structures such as pyramids and grooved structures required in nanophotonic applications[18]. In this article, we report the synthesis and microscopy characterization of pentagonal bipyramidal structures of Au which are typically $\sim$10 μm long. We also demonstrate how individual microcrystals can be employed as SERS substrates and optical waveguides.

Anisotropic structures of Au reported in the literature are usually obtained *via* solution phase synthesis, upon reduction of metal ions stabilized with a suitable surfactant, in the presence of Ag(I) ions[6,19]. The latter is understood to play a key role in producing high index planes resulting in interesting morphologies[20,21]. Nevertheless, these are seed-mediated multistep reactions[22] employing high concentrations of surfactants[23] or highly acidic conditions[8] to control the growth. The method, presented in this article, makes use of Ag(I) but not in solution phase. It is

essentially a simple, single step solid state synthesis on a flat substrate, in which a precursor, i.e., a mixture of Au(III) and Ag(I) stabilised by tetraoctylammonium bromide (ToABr) named as AuAgToABr, is subjected to thermolysis on a hot plate in air, to produce long corrugated pentagonal bipyramidal microcrystals.

The background, which led to this recipe, is interesting. Recently, some of us reported the synthesis of single crystalline Au microplates by the thermolysis of Au(III) stabilised with ToABr (AuToABr) (see Supplementary Fig. S1 online)[24]. Similar attempts with AgToABr led to AgBr (see Supplementary Fig. S2 online), as Ag-Br formation is thermodynamically more favourable than of Ag-Ag[25]. We considered it interesting to examine if Ag(I) will have an influence on Au(III) reduction to form alloy nanostructures. We therefore prepared mixed precursors (AuAgToABr) by phase transferring Au(III) and Ag(I) ions simultaneously from aqueous to organic medium i.e., toluene (see Methods and Supplementary Fig. S3 online). Upon drop coating a mixed precursor (75 : 25 of Au(III) : Ag(I)) on a Si substrate and thermolyzing in air (see schematic in Fig. 1a), there were no plate-like structures but instead micron sized long structures and symmetric 3D particles were obtained along with AgBr particles. The latter could be washed away by treating with liquor ammonia (see Supplementary Fig. S4 online). The focus of the present study is on the long micron sized anisotropic structures.

Results

Optimization of synthesis conditions. As shown in the scanning electron microscopy (SEM) image in Fig. 1b, the obtained structures are 10 ± 2 μm long. The central diameter was found to be in the range, 0.9–1.15 μm with a typical aspect ratio of ~7 (see histogram in Fig. S5). The magnified images in Figs. 1c, d and e bring out the interesting morphology of the long structures. They are tapered on both sides, from the center to the tips and the tapering is not smooth but corrugated. The tips are sharp with a radius of curvature of ~55 nm and a tip angle of ~30° (Figure 1d). The contiguous corrugated features appear akin to folded fingers (Figure 1e). A side view reveals that the corrugated steps are approximately arranged in a pentagonal symmetry (Figure 1f) along the long axis. We term these interesting structures as micron sized corrugated pentagonal bipyramids (μ-CPBs). Atomic force microscopy (AFM) topography image (Figure 1g) shows a well-defined stepped surface which is reflected in the height profile shown in Fig. 1h. The width of the steps varied from ~180 nm at the tip to ~675 nm at the center. The surface roughness on the flat regions of μ-CPB was minimal i.e., ~1.5 nm (see Supplementary Fig. S6 online). It is of considerable importance to have minimal surface roughness to alleviate the loss in light propagation studies[18].

The morphology of μ-CPBs and their relative population to other 3D particles depend on the Au(III) : Ag(I) ratio in the precursor as well as on the thermolysis temperature (Fig. 2). Elongated structures were observed when Au(III) : Ag(I) = 90 : 10 ratio was employed (Fig. 2a). They appear as dumbbells with pentagonal symmetry with flattened smooth edges; and the average length was found to be ~3 μm. The average length increased to ~3.5 μm with 80 : 20 of Au(III) : Ag(I) and the elongated structures (see Fig. 2b) resembled
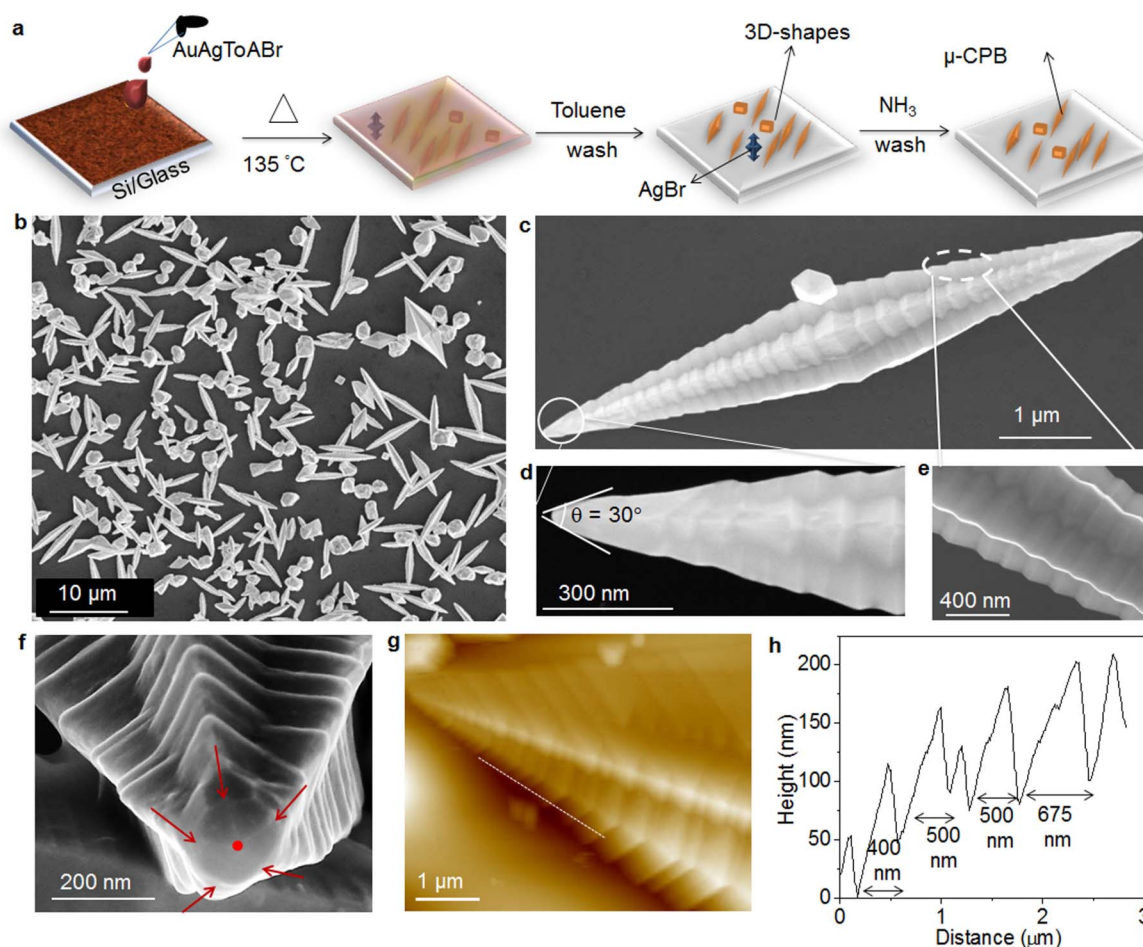

Figure 1 | SEM images and surface characterization of μ-CPBs. (a) Schematic illustrating the synthesis of μ-CPBs. SEM images of μ-CPBs prepared at 135°C for 75:25 of Au(III) : Ag(I) – (b) low magnification, (c) single μ-CPB, (d) magnified view of the tip and (e) side facets marked in (c). (f) High resolution image of the pentagonal symmetry at the tip. (g) AFM topography image of the stepped surface of a μ-CPB and (h) height profile along the line drawn in (g).
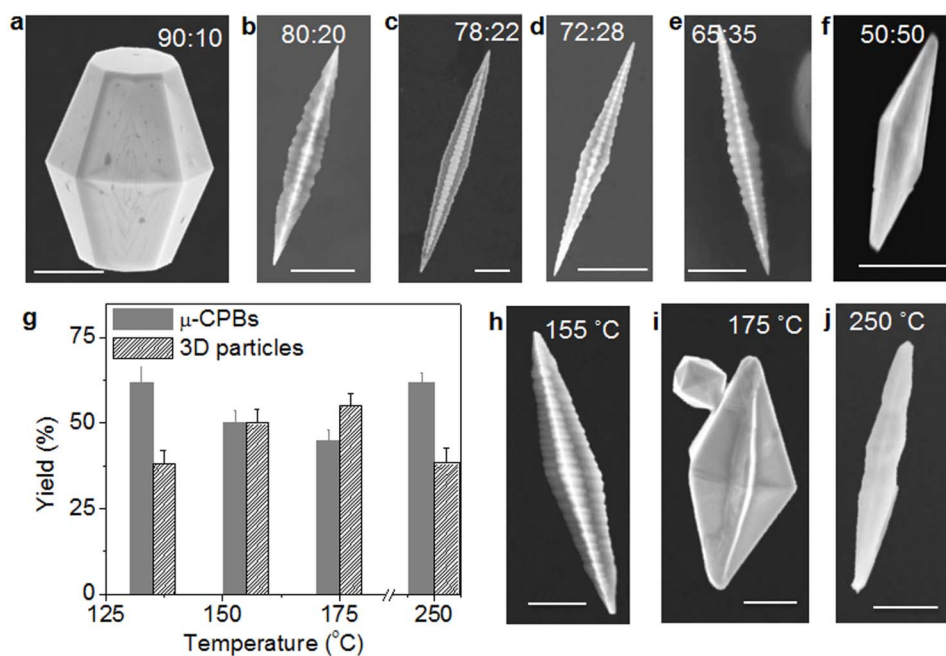
Figure 2 | Optimization of size and shape of μ-CPBs. (a–f) SEM images of μ-CPBs prepared with different mole ratios of Au(III) and Ag(I) at 135°C. (g) Histograms showing the relative populations of μ-CPBs and 3D particles obtained for various thermolysis temperatures (Au(III) : Ag(I) ratio, 75 : 25). Error bars represent standard deviations in the yields. (h–j) SEM images of μ-CPBs obtained at various thermolysis temperatures. All scale bars correspond to 1 μm.

closely μ-CPBs obtained with the 75 : 25 ratio (Fig. 1c). The surface morphology was found to be sensitive in this concentration region (see Fig. 2c–e). At 50 : 50, the pentagonal bipyramids possess small length (1.5 μm) with smooth surface (Fig. 2f). From the above experiments, it is clear that 75 : 25 of Au(III) : Ag(I) produced the longest particles (μ-CPBs) with well-developed corrugations. It is noteworthy that the μ-CPBs produced in this study are distinct from the nanorice/bipyramidal particles reported in the literature[26,5,7], the latter being typically sub-μm in length. As μ-CPBs are few micrometers in length, they can be easily visualized and manipulated under a conventional optical microscope (see Supplementary Fig. S7 online) unlike the nanorice/bipyramids.

Besides the metal content, thermolysis temperature was found to be a crucial parameter for controlling the structure of μ-CPBs. The histogram in Fig. 2g shows the relative yields of μ-CPBs and 3D structures as a function of thermolysis temperature. μ-CPBs yield is above 45% at all temperatures. The thermogravimetric analysis indicates that there is no weight loss below 135°C and the precursor decomposition is rapid above 170°C (see Supplementary Fig. S8 online). The length and morphology of μ-CPBs are influenced by the rate of precursor decomposition; slower the decomposition, longer the μ-CPBs. At 135°C and 155°C, we observed long μ-CPBs with sharp tips (see Fig. 1 and 2h respectively), while short pentagonal bipyramids with blunt tips and smoother surfaces are seen at higher temperatures (see Fig. 2i and j). The ones observed at 175°C (see Fig. 2i) are bipyramids which possess similar morphology as reported in ref 15. The μ-CPBs prepared at 250°C (see Fig. 2j) resemble the nanorods morphology reported in the literature[26]. Thus, higher growth kinetics does not seem to permit the formation a well corrugated surface. A higher reduction rate at elevated temperatures leads to large number of nucleation sites and in turn, a large number of smaller particles.

Structure of μ-CPB. In order to understand the structure of the μ-CPBs in detail, high resolution X-ray diffraction (XRD), SEM and transmission electron microscopy (TEM) analysis have been performed. The μ-CPBs are highly crystalline as evident from the

XRD pattern. The intensity of the (220) peak was found to deviate from the standard JCPDS data (65–2870) by 44% (see Supplementary Fig. S4 online), as <110> is the preferred growth direction. Low magnification TEM image (Figure 3a) shows the corrugated surface of a μ-CPB. Electron diffraction (ED) pattern collected from the tip showed two sets of spots (see Fig. 3b), hexagonal and rhombus patterns overlapping each other. These correspond to the Au FCC lattice viewed along the <111> and <110> zone axes, respectively. The ED pattern from the center of μ-CPB also shows two sets of spots indexable to <112> and <001> zone axes (see Fig. 3c). Similar ED patterns have been observed in the case of penta-twinned Au, Ag and Cu nanorods[27]. This indicates that the μ-CPBs possess a penta-twinned structure grown along the <110> direction. When high resolution TEM (HRTEM) was performed at the tip, the observed spacing between the fringes was ~2.36 Å corresponding to a d-spacing of Au(111) (see Fig. 3d). Figure 3e shows HRTEM image collected from the region of the side facets of μ-CPBs (indicated as e in Fig. 3a). The d-spacing was ~2.07 Å corresponding to Au(200). The zig-zag ridges cannot be the (100) planes as the latter are atomically flat. The values of the angles at the ridges point to plausible existence of high-index planes. From the TEM image (Fig. 3f), the angles subtended by the surface planes of the adjacent ridges are measured to be 147.1° and 146.8°, which are in close agreement with expected angular relation for the (730) and (610) (∠a = 147.3°) and, (210) and (910) (∠β = 147.09°) (see Supplementary Table S2 online). To further confirm the assignments, one may refer to the projection angles in edge-on orientation along the <110> axis (see supplementary Table S2 online and Fig. 3g). Considering the ridges to be extraneous growth from the atomically flat (100) planes, the measure edge-on projection angles indicate that the ridges are {hk0} (see Supplementary Tables S2 and S3 online and Figs. 3f, 3g) (where h>1 and k ≥ 1) type high-index planes[7]. Based on the above results, the growth direction of the μ-CPBs is considered to be <110> while the side facets are (100). The tips are enclosed with stable {111} facets, in agreement with the reported literature on Au nanorice[5,7]. Figure 3h shows a highly magnified SEM image of a
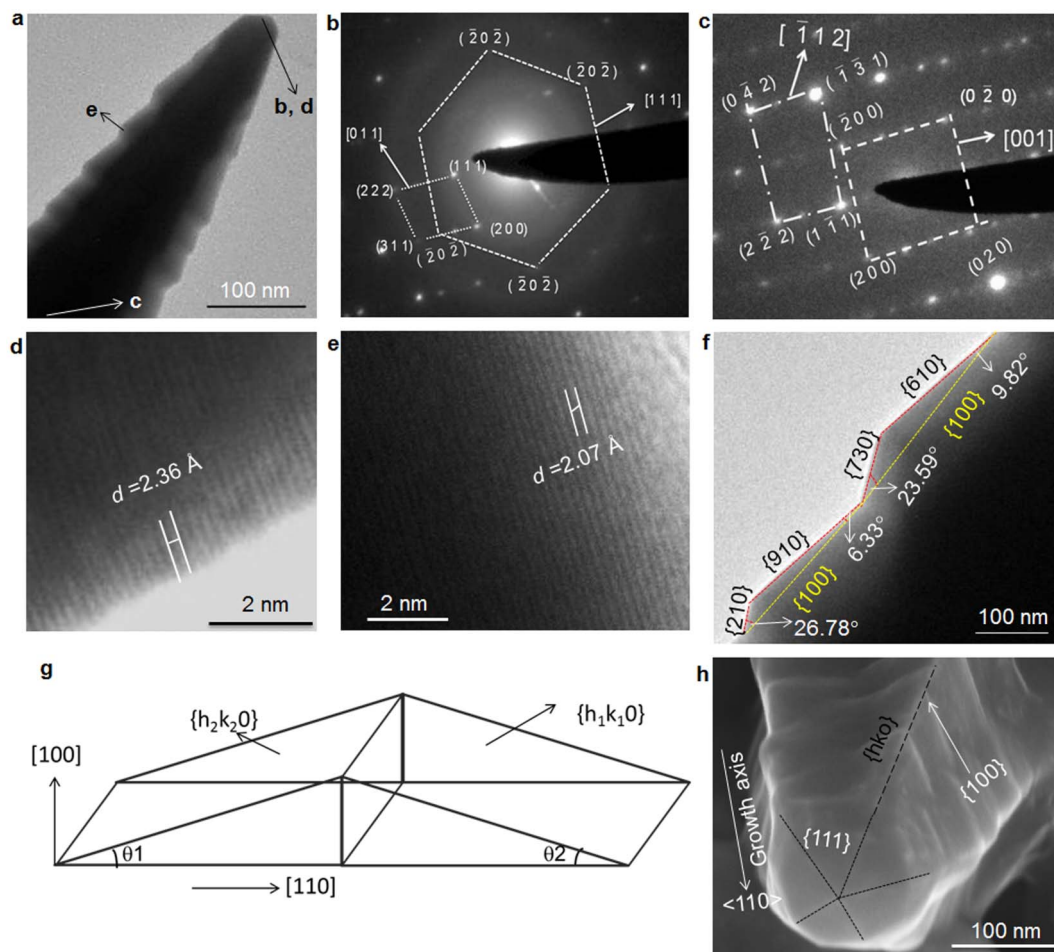
Figure 3 | TEM characterization. (a) TEM image of μ-CPB showing corrugated steps. ED patterns from μ-CPB's (b) tip and (c) center are shown. HRTEM images from the (d) tip and (e) side edges of μ-CPBs are shown along with the d-spacings marked corresponding to (111) and (200) respectively. (f) Magnified TEM image of a μ-CPB, showing ridges made of {hk0} type high index facets. (g) A schematic illustration of a ridge bound by high index facets and (h) a magnified SEM image of a μ-CPB with the facets indexed.

μ-CPB with various planes and growth directions assigned, based on ED and HRTEM analysis. The surface composition of μ-CPBs was examined using core-level spectroscopy (see Supplementary Fig. S9 online). Interestingly, the surface was found to be almost entirely made of Au(0), Ag(0) being negligible.

Growth mechanism. The growth of μ-CPBs is indeed interesting. A μ-CPB has two growth modes namely along the longitudinal axis and the lateral growth leading to the observed corrugation (five-fold stars stacked along the longitudinal growth direction). These aspects were investigated by arresting the growth of μ-CPBs at different time periods by simply removing the substrate from the hot plate and examining under SEM. Initially, we discuss the growth along <110> direction. The thermolysis carried out for 30 min gave rise to nearly spherical particles in the range, 25–30 nm (see Supplementary Fig. S10 online). The particles may have definite facets which is however not clearly visible in the SEM images owing to their small size. The facets become visible once the particles grew beyond 100 nm (time of thermolysis, 60 min). At this point, the particle is essentially a multiply twinned decahedron (MTD) (see Fig. 4b and its schematic in Fig. 4a) which is one among the known stable polyhedrons in this size regime[28]. It has ten {111} facets, five {100} facets and two possible growth directions, <110> i.e., along the particle axis and also along five equivalent <112> directions across the particle side faces[29] as shown in Fig. 4a. Anisotropic particle growth is mainly due to the differences in the

growth rates on different crystallographic facets. For FCC metals, the surface energy of different facets is as follows, $\gamma_{(111)} < \gamma_{(100)} < \gamma_{(110)}$. The {110} and {211} faces have surface energies of 0.0991 and 0.0908 eV/$\mathring{A}^{-2}$ respectively. Hence a faster growth along the <110> direction is expected[30]. The growth rate along the <112> direction comes next[29]. There is another contributing factor for the anisotropic structure of the μ-CPB. MTD is viewed as an association of five tetrahedral units, sharing an edge. The angle expected between two tetrahedral units is 70.53°. When five such tetrahedrons are stacked in a face-to-face orientation, there will be an angular gap of 7.35° to fill in[31]. It therefore causes strain at the corners, which in turn induces anisotropic growth of μ-CPBs. MTD may act as a seed for further growth and this aspect is discussed in detail in the literature in relation to Au/Ag anisotropic structures[32]. In the given reaction mixture, the following reactions are expected where the described redox potentials are with respect to the standard hydrogen electrode (SHE).

$$Ag(0) \rightarrow Ag(I) + e^- \qquad E_0 = -0.8 \text{ V} \qquad (1)$$

$$Ag + Br^- \rightarrow AgBr + e^- \qquad E_0 = 0.3 \text{ V} \qquad (2)$$

$$Au(III) + 3e^- \rightarrow Au(0) \qquad E_0 = 0.99 \text{ V} \qquad (3)$$

Following equations 1 and 2, Ag(0) oxidizes to Ag(I) and generates an electron[33,34]. Au ions get reduced by accepting the electrons according to equation 3. It is therefore not surprising that no
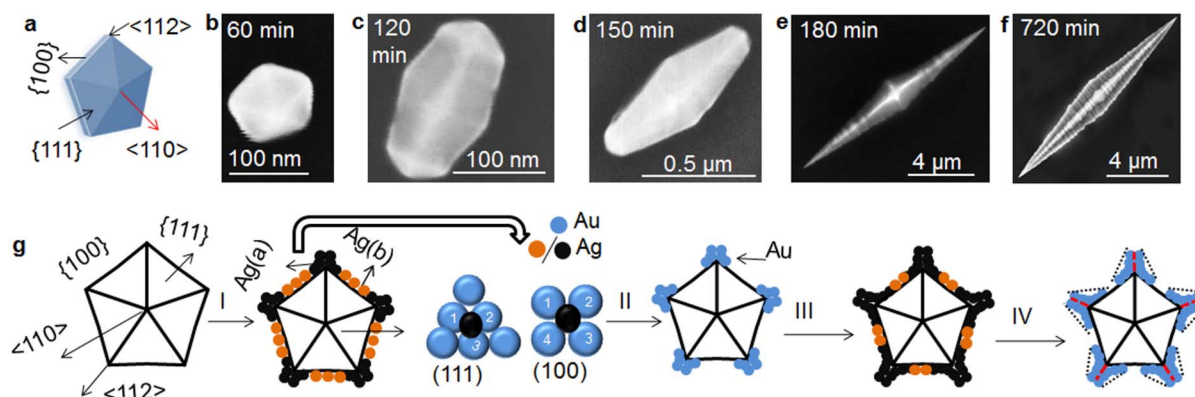
4

Figure 4 | Investigation of growth of μ-CPBs. (a) Schematic of decahedron with facets and growth directions marked. (b–f) FESEM images of typical μ-CPBs collected at different time periods during thermolysis at 135°C. (g) Schematic depicting growth along <112> directions involving Ag(I) deposition on Au facets and galvanic displacement of Ag(0) by Au(I) from the surrounding molten precursor. This process eventually leads to the fivefold star shape as seen along the <110> direction.

significant Ag3d signal was observed in X-ray photoelectron spectrum (XPS) (see Supplementary Fig. S9 online).

As shown in Fig. 4c, nanoparticles obtained at 120 min thermolysis appear like elongated decahedrons. Similar structures are addressed as nanorice in the literature. They have a typical length of ~150 nm and an aspect ratio ~2. In the subsequent growth, the aspect ratio of the decahedron increased by many folds (see Fig. 4d corresponding to 150 min thermolysis). In stage 4d, the nanoparticles became tapered with a large curvature. The intense electric field associated at the tip helps rapid reduction of Au(I) and Au(III) at the tip[35], favoring the tapered growth. Also, the electron liberated from Ag oxidation (see equations 1 and 2) moves to the tip of the μ-CPB particle, which leads to reduction of Au ions present in the reaction medium at the tip (see equation 3)[7]. These processes lead to a relatively fast kinetics for longitudinal growth, thus eventually forming μ-CPBs (see SEM images in Figs. 4e and f). This is clear from the histogram in Fig. S11, which shows the mean length of μ-CPBs as a function of growth time.

The discussion below is related to the growth of μ-CPB along the <112> direction. On the decahedron, the strained corners act as reactive sites to generate ridges-like extra growth. As shown in Fig. 4g, the twin planes are oriented in the <112> direction. Ag(I) from precursor deposits preferentially on the Au{100} facets due to its lower deposition potential. On this plane, Ag finds higher coordination than on {111}[6] (see Fig. 4g). Ag(0) present on the Au{100} facets (indicated by brown colored circles in Fig. 4g) could be oxidized by a bromide ion present in the reaction mixture, leading to discharge of an electron (equation 2)[7] and release of AgBr. On the other hand, Ag(0) present at the boundary line where {100} facets meet (shown as black circles in Fig. 4g), gets galvanically displaced by Au(I) and thus stabilizes the energetic twin plane[36]. This may lead to the growth of a star shape from a decahedron. The deposition and dissolution of Ag and the galvanic displacement of Au along the <112> directions take place repeatedly to produce well-defined star shaped Au petals on a decahedron base. These ridges are high index planes as shown in the TEM analysis (see Fig. 3f). Growth mechanism along the <112> direction is shown in Fig. 4g. The ridges along the <112> directions are the corrugated structures observable from the top view of the μ-CPBs (for SEM images, see Supplementary Fig. S12 online). Growth along the <110> and <112> contribute simultaneously to produce longer pentagonal bipyramids with corrugated surfaces. Ultra-slow precursor decomposition at 135°C is also an important contributing factor. At higher temperatures, the differences in the growth rates in different directions may be small. The ten {111} facets at the tip remain almost unaffected from the seed decahedron to μ-CPBs as the growth on these planes is

thermodynamically unfavorable. The longitudinal growth along the growth axis is relatively rapid whereas the side facets i.e., {100} are adsorbed with Ag which acts as a surfactant and thus the growth is inhibited.

While Ag actively participates in the Au μ-CPBs growth, it does not become part of it (see Supplementary Fig. S9 online). Following the Hume–Rothery rules[37], one would expect an alloy formation, as Ag has similar lattice parameters. Not quite surprisingly, Au-Ag alloy bipyramids (40–90 nm) have been reported in the literature starting with HAuCl₄, AgNO₃ and polyvinylpyrrolidone (PVP) as a capping agent[38]. In the present method, clearly, Au and Ag though exist in *atomic intimacy*, did not form an alloy. The reason for this unusual behavior is that the Au and Ag precursors separate themselves into different domains as the solvent evaporates from the mixed precursor, prior to thermolysis. This became apparent from XRD patterns and polarizing microscopy images (see Supplementary Fig. S13 online) collected from the precursor film, which showed AuToABr and AgToABr crystallizing in individual domains. This may be an additional parameter contributing to the observed highly anisotropic growth.

By virtue of such contributing factors at play, remarkably large multiply twinned particle (MTP) structures (Au μ-CPBs) have thus been observed which stand out from the known aniosotropic structures till date. The MTP structures reported in literature are usually nanoparticles with decahedron or slightly elongated rice morphology else nanowires with five-fold tapered ends. The μ-CPB particles reported here are unique in that the tips are made of MTP structure while the deeply corrugated surface is covered with high index facets. Large sized, micrometer to millimeter, MTP structures are not commonly reported in the literature. Penta twinned micron/millimeter size decahedrons and its derivative structures have been found under highly acidic conditions[39] but with little yield. Occasionally, they may be found in nature as well[40]. Thus, the results presented here are of immense significance.

SERS, pick and probe measurements. The corrugated surface of the μ-CPB prompted us to use them as SERS substrates. For this purpose, thiophenol (TP) (1 mM) and Rhodamine 6G (R6G) (1 mM) were used as Raman probe molecules. The Raman spectrum of TP recorded on an individual μ-CPB shown in Fig. 5a, consists of intense peaks at 1000, 1023, 1070 and 1576 cm⁻¹, all assignable to various vibration modes in ring breathing, C-H bending, C-S stretching and C=C bond respectively of the aromatic ring[41]. The Raman enhancement factor (G) calculated based on the peak intensity at 1576 cm⁻¹ is found to be 2.4 × 10⁶ for TP. In the spectrum shown in Fig. 5b, the peaks are assignable to R6G

vibrational modes; peak at 614 cm^{-1} corresponding to C-C-C stretching mode and the peaks at 1355 and 1509 cm^{-1} stand for the C-C stretching[42]. Enhancement factor (also known as G-factor) is estimated to be 5.8 × 10^6 based on the peak at 614 cm^{-1}.

Since μ-CPBs are sharp objects, we tried pick and probe technique for molecules using single μ-CPB. A polymer (PVP) film containing probe molecules (R6G) was chosen, which was gently scratched with a μ-CPB mounted on a Cu wire using a micromanipulator (see Supplementary Fig. S14 online and Figs. 5d–g). A small amount of R6G-PVP blend was thus picked up on the μ-CPB tip. The spectrum collected from the tip of μ-CPB (see Fig. 5c) is relatively noisy and the peaks are broadened due to the inhomogeneous environment[43] of the analyte molecules on the μ-CPB surface. The number of adsorbed R6G molecules on the tip estimated based on the area of μ-CPB tip came out to be ~2700. The above experiment illustrates the possibility of using μ-CPBs in sensitive SERS based detection. Unlike conventional plasmonic nano-crystals, these microcrystals exhibit broad plasmon spectral features and have excitations at both visible and infra-red wavelengths (see Supplementary Fig. S15 online). Further, they host nanoscale topographic features in the form of ridges which form interesting sites for adsorption of molecules. Indeed, such confined nano-volumes act as plasmonic hot-spots where large electric fields can build up giving rise to enhanced light-molecule interaction such as SERS.

Light propagation. The μ-CPBs were investigated for light propagation as they have corrugated, grating-type surface with minimal roughness at each step as well as tapered ends resembling tapered V-grooves[44]. These structural features are important because the tips can facilitate localized optical fields while the corrugations on the surface facilitate effective conversion of free photons to surface plasmons with minimal scattering loss[45]. With this hindsight, we tested the plasmon assisted light propagation properties of Au μ-CPBs. Figure 6a shows the dark-field optical image of an isolated Au μ-CPB. Upon focusing a 632.8 nm (2 μm diameter) laser beam on one end of the Au μ-CPB (Figure 6b), we observed out-coupling of light at the distal end of the microstructure. This clearly indicated that the μ-CPB acts as a plasmonic waveguide. The incidence of visible light at one end of the structure causes the conversion of momentum of free photons into that of propagating plasmon polariton within the microstructure. This propagating plasmon reaches the distal end of the μ-CPB where again the plasmon polaritons are back-converted into free photons (see Figs. 6b and c).

In order to quantify the performance of μ-CPBs as plasmon wave-guides, we calculated the propagation loss in the structure. Propagation loss (α) is given by[46]

$$\alpha = (-10 \times \log(1/e))/L_0 = 4.343/L_0 \qquad (4)$$

where L_0 is the propagation length, calculated using the formula

$$I(x) = I_0 \times \exp(-x/L_0) \qquad (5)$$

where I_0 is the incident intensity, $I(x)$ is the intensity out-coupled light at distance x from the incident spot. For the Au μ-CPB of length 8.8 μm shown in Fig. 6a, the calculated propagation loss was 2.32 dB/μm. The propagation loss in the microstructure is both radiative and ohmic. The nanoscale ridges may scatter the plasmon resulting in photon emission. One way to overcome the losses is to use smooth bipyramid-like structures (Fig. 2a), and further taper them down with a focused-ion beam or possibly by a chemical recipe. This will facilitate nano-tapered, single crystalline, low-loss plasmonic structures that can be utilized for efficient optical waveguiding. It is to be noted that ridges in our geometry do have an advantage as
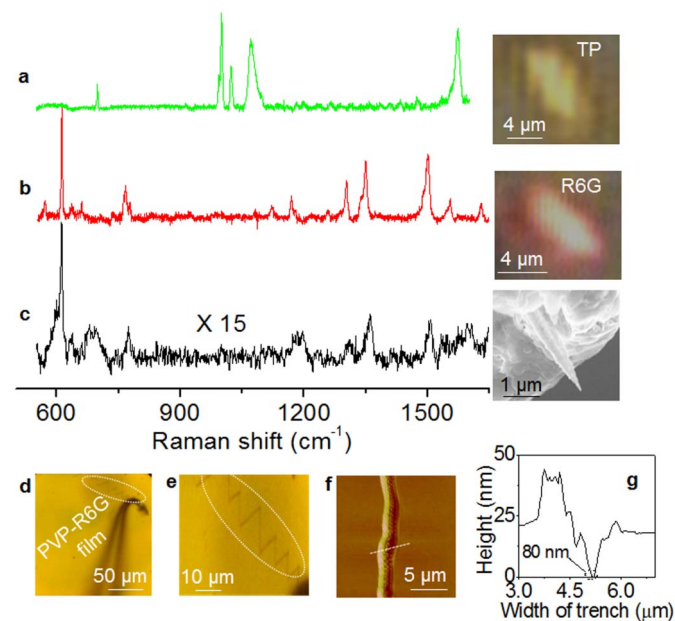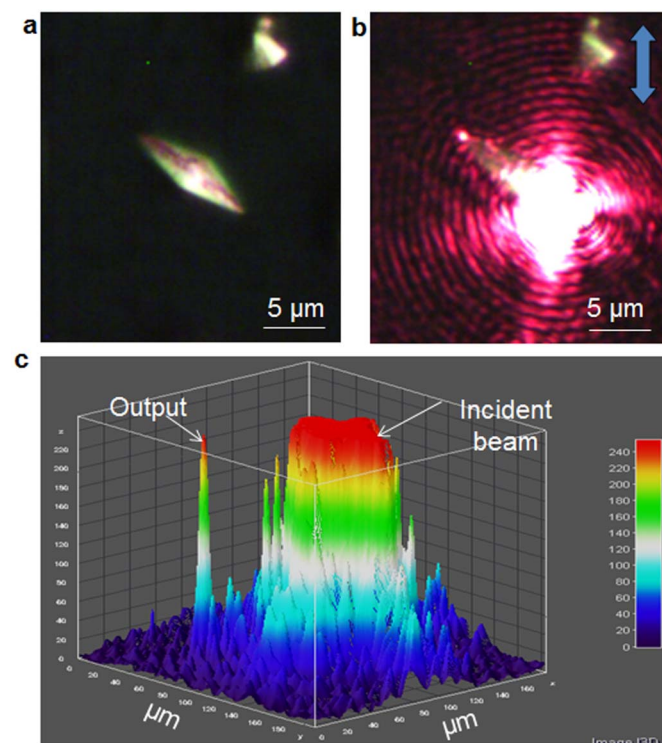

Figure 5 | SERS, picking the analyte and probing. Raman spectra recorded from single μ-CPB adsorbed with the probe molecules; (a) thiophenol (TP) and (b) rhodamine 6G (R6G). The optical images from the Raman spectrometer images are shown on the right. The μ-CPB particles were located on a glass substrate after treatment with the TP/R6G solutions. In another experiment, a PVP-R6G blend deposited as a film on glass substrate was poked with the tip of a μ-CPB and the Raman spectrum (c) was recorded from the tip region. The corresponding SEM image is shown on the right. Manipulation of μ-CPBs was done using a thin Cu wire. Optical microscopy image in (d) shows a zigzag scratch (marked by white boundary) on the film with a magnified view in (e). (f) AFM image of the scratched line and (g) its height profile.

Figure 6 | Light propagation. (a) Dark-field optical image of a μ-CPB. (b) Plasmon assisted light propagation at incident wavelength of 632.8 nm, the arrow indicates the polarization of the focused laser beam. (c) Three-dimensional projection of the image in b showing the incident beam and the out-coupled light at the distal end of the μ-CPB.

they can act as periodic hot-spots. Therefore, molecules confined to these ridges are subject to large electric fields. This can be further harnessed for sensitive detection of molecules at ultra-low concentrations. Furthermore, these microcrystals with controllable nanoscale features can be easily accessed and probed using far-field optical microscopy techniques. This is a major advantage when one needs to interface such structures with biological entities such as cells and tissues.

Discussion

In conclusion, μ-CPBs were synthesized using a simple solid state synthesis route (i.e., unaided by any solvent). The current method is versatile in that it is a single step synthesis and can be carried out on almost any flat substrate that can withstand 130°C with almost no organic impurities in the final product. The growth of μ-CPBs can be halted or resumed any time, by simply turning on and off the hot plate. The μ-CPBs being long enough can be easily observed using an ordinary optical microscope. Although the μ-CPBs are entirely made of Au, the presence of $(AgBr_2)^-$ ion in the reaction medium seems to play a key role in tuning the shape of the anisotropic particles. Shape and size of the μ-CPBs can be tailored by varying the mole ratio of Au(III) and Ag(I) in the precursor as well as by the thermolysis temperatures. The μ-CPBs serve as excellent SERS substrates. The efficiency of the tip of a μ-CPB was studied in a *"pick and probe experiment"*. The tip carrying only 2700 R6G molecules produced a measurable Raman signal. The tapered structure of μ-CPB facilitates concentration of the light at the tips with a propagation loss of 2.32 dB/μm. Conventionally plasmonic nanoparticles that occupy small volumes are used for localized surface plasmon resonance, and one dimensional elongated structures such as plasmonic wires are utilized for optical waveguiding properties. The uniqueness of the geometry studied herein is that it can facilitate both localized and propagating plasmons on a single platform. As a 'proof-of-concept', we have shown that the prepared nanostructures can be harnessed for both surface enhanced Raman scattering which is a property based on localized plasmons, and plasmon-assisted optical waveguiding which is based on propagating plasmon-polaritons. While the focus of the present study is on one anisotropic structure, the approach need not necessarily be limited; such synthetic routes involving single source precursors hold great promise for the synthesis of exotic anisotropic materials.

Methods

Chemicals and synthesis of AuAgToABr. Hydrogen tetrachloroaurate(III) hydrate ($HAuCl_4.3H_2O$), silver nitrate ($AgNO_3$), tetraoctylammonium bromide (ToABr), and toluene were obtained from spectrochem, India and used without further purification. Water used throughout this investigation was double distilled. To a 1.5 mL of $HAuCl_4$ (25 mM), 6 mL of tetraoctylammonium bromide (ToABr) in toluene (50 mM) was added and stirred for 5 min[48]. The bottom aqueous phase became colorless and top organic phase developed red color. Then, a 0.5 mL of $AgNO_3$ (25 mM) was added to the solution and stirred for ~10 hrs. In this case, the mole ratio of Au(III) and Ag(I) in aqueous phase was 75 : 25. Likewise, different mole ratios of Au(III) and Ag(I) such as 50 : 50, 65 : 35, 80 : 20, 90 : 10 have been prepared. In all the experiments, the volume ratio of aqueous and organic phase was kept constant at 1 : 3. Freshly prepared solution was used for growth of μ-CPBs. The substrates used i.e., Si and glass were cleaned twice with water, IPA, toluene and dried under N_2 gas.

Characterization. Scanning electron microscopy (SEM) was performed using a Nova NanoSEM 600 equipment (FEI Co., The Netherlands). Energy dispersive spectroscopic (EDS) mapping was performed using EDAX Genesis V4.52 (USA) attached to the SEM column. Atomic force microscopy (AFM) experiments were carried out using Bruker diInnova Scanning Probe Microscope with Nanodrive controller. Imaging has been done in tapping Mode. Transmission electron microscopy measurements were carried out with a JEOL-3010 instrument operating at 300 kV (λ = 0.0196 Å). XRD measurements were performed on a Miniflex (Rigaku, Japan) (Cu Kα, 1 × 5406 Å; scan rate, 1 deg/min). Plasmon assisted light propagation of individual Au μ-CPB was tested on an upright microscope (Olympus BX51) with dark-field and bright-field illumination modules and a CCD camera. He-Ne laser at 632.81 nm was focused through a 50×, 0.5 NA (long working distance) objective lens on one of the ends of the Au μ-CPB and the resultant image was captured using CCD and processed using ImageJ 3D software. The details of the optics can be found elsewhere[47].

1. Murphy, C. J. et al. Anisotropic Metal Nanoparticles: Synthesis, Assembly, and Optical Applications. *J. Phys. Chem. B* **109**, 13857–13870 (2005).
2. Tao, A. et al. Langmuir-Blodgett Silver Nanowire Monolayers for Molecular Sensing Using Surface-Enhanced Raman Spectroscopy. *Nano Lett.* **3**, 1229–1233 (2003).
3. Yu Chang, S.-S., Lee, C.-L. & Wang, C. R. C. Gold Nanorods: Electrochemical Synthesis and Optical Properties. *J. Phys. Chem. B* **101**, 6661–6664 (1997).
4. Xia, Y., Xiong, Y., Lim, B. & Skrabalak, S. E. Shape-Controlled Synthesis of Metal Nanocrystals: Simple Chemistry Meets Complex Physics? *Angew. Chem. Int. Ed.* **48**, 60–103 (2009).
5. Kou, X. et al. Growth of Gold Bipyramids with Improved Yield and Their Curvature-Directed Oxidation. *Small* **3**, 2103–2113 (2007).
6. Liu & Guyot-Sionnest, P. Mechanism of Silver(I)-Assisted Growth of Gold Nanorods and Bipyramids. *J. Phys. Chem. B* **109**, 22192–22200 (2005).
7. Zheng, Y. et al. Facile Synthesis of Gold Nanorice Enclosed by High-Index Facets and Its Application for CO Oxidation. *Small* **7**, 2307–2312 (2011).
8. Pelton, M. et al. Damping of acoustic vibrations in gold nanoparticles. *Nat. Nanotechnol.* **4**, 492–495 (2009).
9. Burgin, J., Liu, M. & Guyot-Sionnest, P. Dielectric Sensing with Deposited Gold Bipyramids. *J. Phys. Chem. C* **112**, 19279–19282 (2008).
10. Rodríguez-Lorenzo, L., Álvarez-Puebla, R. N. A., de Abajo, F. J. G. A. & Liz-Marzán, L. M. Surface Enhanced Raman Scattering Using Star-Shaped Gold Colloidal Nanoparticles. *J. Phys. Chem. C* **114**, 7336–7340 (2009).
11. Liu, N., Tang, M. L., Hentschel, M., Giessen, H. & Alivisatos, A. P. Nanoantenna-enhanced gas sensing in a single tailored nanofocus. *Nat. Mater.* **10**, 631–636 (2011).
12. Hasan, W. et al. Tailoring the Structure of Nanopyramids for Optimal Heat Generation. *Nano Lett.* **9**, 1555–1558 (2009).
13. Liang, H., Yang, H., Wang, W., Li, J. & Xu, H. High-Yield Uniform Synthesis and Microstructure-Determination of Rice-Shaped Silver Nanocrystals. *J. Am. Chem. Soc.* **131**, 6068–6069 (2009).
14. Vigderman, L. & Zubarev, E. R. Starfruit-Shaped Gold Nanorods and Nanowires: Synthesis and SERS Characterization. *Langmuir* **28**, 9034–9040 (2012).
15. Senapati, D., Singh, A. K. & Ray, P. C. Real time monitoring of the shape evolution of branched gold nanostructure. *Chem. Phys. Lett.* **487**, 88–91 (2010).
16. Ropers, C. et al. Grating-coupling of surface plasmons onto metallic tips: A nanoconfined light source. *Nano Lett.* **7**, 2784–2788 (2007).
17. Lindquist, N. C., Nagpal, P., Lesuffleur, A., Norris, D. J. & Oh, S.-H. Three-Dimensional Plasmonic Nanofocusing. *Nano Lett.* **10**, 1369–1373 (2010).
18. Nagpal, P., Lindquist, N. C., Oh, S.-H. & Norris, D. J. Ultrasmooth Patterned Metals for Plasmonics and Metamaterials. *Science* **325**, 594–597 (2009).
19. Kou, X. et al. Growth of Gold Nanorods and Bipyramids Using CTEAB Surfactant. *J. Phys. Chem. B* **110**, 16377–16383 (2006).
20. Ming, T. et al. Growth of Tetrahexahedral Gold Nanocrystals with High-Index Facets. *J. Am. Chem. Soc.* **131**, 16350–16351 (2009).
21. Personick, M. L., Langille, M. R., Zhang, J. & Mirkin, C. A. Shape Control of Gold Nanoparticles by Silver Underpotential Deposition. *Nano Lett.* **11**, 3394–3398 (2011).
22. Wu, H.-L., Chen, C.-H. & Huang, M. H. Seed-Mediated Synthesis of Branched Gold Nanocrystals Derived from the Side Growth of Pentagonal Bipyramids and the Formation of Gold Nanostars. *Chem. Mater.* **21**, 110–114 (2008).
23. Lee, S., Mayer, K. M. & Hafner, J. H. Improved Localized Surface Plasmon Resonance Immunoassay with Gold Bipyramid Substrates. *Anal. Chem.* **81**, 4450–4455 (2009).
24. Radha, B., Arif, M., Datta, R., Kundu, T. & Kulkarni, G. Movable Au microplates as fluorescence enhancing substrates for live cells. *Nano Res.* **3**, 738–747 (2010).
25. deB. Darwent, B. Bond Dissociation Energies in Simple Molecules. http://www.nist.gov/data/nsrds/NSRDS-NBS31.pdf (1970).
26. Zhou, Z.-Y., Tian, N., Huang, Z.-Z., Chen, D.-J. & Sun, S.-G. Nanoparticle catalysts with high energy surfaces and enhanced activity synthesized by electrochemical method. *Faraday Discuss.* **140**, 81–92 (2009).
27. Johnson, C. J., Dujardin, E., Davis, S. A., Murphy, C. J. & Mann, S. Growth and form of gold nanorods prepared by seed-mediated, surfactant-directed synthesis. *J. Mater. Chem.* **12**, 1765–1770 (2002).
28. Elechiguerra, J. L., Reyes-Gasga, J. & Yacaman, M. J. The role of twinning in shape evolution of anisotropic noble metal nanostructures. *J. Mater. Chem.* **16**, 3906–3919 (2006).
29. Tsuji, M. et al. Toward to branched platinum nanoparticles by polyol reduction: A role of poly(vinylpyrrolidone) molecules. *Colloids Surf. A* **317**, 23–31 (2008).
30. Kan, C. et al. Gold Microplates with Well-Defined Shapes. *Small* **6**, 1768–1775 (2010).
31. Tsuji, M. et al. Stepwise Growth of Decahedral and Icosahedral Silver Nanocrystals in DMF. *Cryst. Growth Des.* **10**, 296–301 (2009).
32. Seo, D. et al. One-Dimensional Gold Nanostructures through Directed Anisotropic Overgrowth from Gold Decahedrons. *J. Phys. Chem. C* **113**, 3449–3454 (2009).
33. Sun, Y. Silver nanowires - unique templates for functional nanostructures. *Nanoscale* **2**, 1626–1642 (2010).
34. Hassan, H. H., Ibrahim, M. A. M., Rehim, S. S. A. E. & Amin, M. A. Comparative Studies of the Electrochemical Behaviorof Silver Electrode in Chloride, Bromide and Iodide Aqueous Solutions. *Int. J. Electrochem. Sci.* **5**, 278–294 (2010).

35. Pérez-Juste, J., Liz-Marzán, L. M., Carnie, S., Chan, D. Y. C. & Mulvaney, P. Electric-Field-Directed Growth of Gold Nanorods in Aqueous Surfactant Solutions. *Adv. Funct. Mater.* **14**, 571–579 (2004).

36. Sławiński, G. W., Ivanova, O. S. & Zamborini, F. P. Twin Plane Decoration of Silver Nanorods with Palladium by Galvanic Exchange at a Controlled Rate. *Langmuir* **27**, 13293–13301 (2011).

37. Raghavan., V. *Materials Science and Engineering: A First Course* Ch. 5 (PHI Learning Pvt. Ltd, New Delhi, 2006).

38. Zhang, X. *et al.* Synthesis and Growth Mechanism of Pentagonal Bipyramid-Shaped Gold-Rich Au/Ag Alloy Nanoparticles. *Langmuir* **23**, 6372–6376 (2007).

39. Gammons, C. H. Hydrothermal synthesis of gold grains with apparent five-fold symmetry. *Can. Mineral.* **34**, 1–8 (1996).

40. Rath, V. Zur Krystallographie des goldes. *Z. Krystallogr.* **1**, 1–17 (1877).

41. Taylor, C. E., Pemberton, J. E., Goodman, G. G. & Schoenfisch, M. H. Surface Enhancement Factors for Ag and Au Surfaces Relative to Pt Surfaces for Monolayers of Thiophenol. *Appl. Spectrosc.* **53**, 1212–1221 (1999).

42. Wang, D.-Y. *et al.* Silver-Nanoparticle-Conjugated Polypeptide Brushes for Surface-Enhanced Raman Scattering. *J. Phys. Chem. C* **113**, 13498–13504 (2009).

43. Kneipp, K., Kneipp, H. & Bohr, H. Topics in Applied Physics (eds Katrin Kneipp, Martin Moskovits & Harald Kneipp) Vol. **103**, 261–277 (Springer Berlin/Heidelberg, 2006).

44. Beermann, J. *et al.* Localized field enhancements in two-dimensional V-groove metal arrays. *J. Opt. Soc. Am. B* **28**, 372–378 (2011).

45. Wild, B. *et al.* Propagation Lengths and Group Velocities of Plasmons in Chemically Synthesized Gold and Silver Nanowires. *ACS Nano* **6**, 472–482 (2011).

46. Ma, Y. *et al.* Direct measurement of propagation losses in silver nanowires. *Opt. Lett.* **35**, 1160–1162 (2010).

47. Chikkaraddy, R., Singh, D. & Kumar, G. V. P. Plasmon assisted light propagation and Raman scattering hot-spot in end-to-end coupled silver nanowire pairs. *Appl. Phys. Lett.* **100**, 043108 (2012).

48. Radha, B. & Kulkarni, G. A Real Time Microscopy Study of the Growth of Giant Au Microplates. *Cryst. Growth Des.* **11**, 320–327 (2011).

Author contributions

G.M., R.B. and G.U.K. designed and performed the experiments and also analyzed the data. D.S. and G.V.P.K. performed light propagation experiments. All authors reviewed the manuscript.

Additional information

Supplementary information accompanies this paper at http://www.nature.com/scientificreports

Competing financial interests: The authors declare no competing financial interests.

How to cite this article: Mettela, G., Boya, R., Singh, D., Kumar, G.V.P. & Kulkarni, G.U. Highly tapered pentagonal bipyramidal Au microcrystals with high index faceted corrugation: Synthesis and optical properties. *Sci. Rep.* **3**, 1793; DOI:10.1038/srep01793 (2013).